Title: Spatiotemporal analysis of elastic and inelastic deformations in roof-rocks from seismological observations

Author: Maciej J. Mendecki, Rafał Pakosz, Łukasz Wojtecki, Wacław M. Zuberek

Citation style: Mendecki Maciej J., Pakosz Rafał, Wojtecki Łukasz, Zuberek Wacław M. (2021). Spatiotemporal analysis of elastic and inelastic deformations in roof-rocks from seismological observations. "International Journal of Mining Science and Technology" (Vol. 31, iss. 2 (2021), s. 241-251), doi 10.1016/j.ijmst.2020.12.001

International Journal of Mining Science and Technology 31 (2021) 241–251

Contents lists available at ScienceDirect

International Journal of Mining Science and Technology

journal homepage: www.elsevier.com/locate/ijmst

Spatiotemporal analysis of elastic and inelastic deformations in roof-rocks from seismological observations

Maciej J. Mendecki [a,*], Rafał Pakosz [b], Łukasz Wojtecki [c], Wacław M. Zuberek [a]

[a] Faculty of Environmental Sciences, the University of Silesia in Katowice, 41-200 Sosnowiec, Poland
[b] Polish Mining Group, 40-039 Katowice, Poland
[c] Central Mining Institute, 40-166 Katowice, Poland

ARTICLE INFO

Article history:
Received 30 July 2020
Received in revised form 3 September 2020
Accepted 6 December 2020
Available online 23 December 2020

Keywords:
Mining seismicity
Seismic source volume
Apparent volume
Hard coal mine
Longwall mining
Benioff strain

ABSTRACT

The spatiotemporal analysis of seismic zones characterised by the scattering and accumulation of strain energy in the roof-rocks of the excavated longwall panel where inelastic or elastic deformations occurred during hard coal seam mining is discussed. The studied longwall panel was designed to utilize the effect of partial stress relaxation caused by the earlier extraction of the coal seams located above. A full seismic moment tensor and spectral source parameter analyses were used to obtain information about the degree of inelastic and elastic coseismic deformations. This study also showed that these deformation changes correspond to variation in the Benioff strain release characteristics. Next, analyses of deformation zones were compared with the relationship between radiated energy and the excavated volume of rocks per month. The concept of balanced seismic energy release assumed the exponential increase of released seismic energy with the increase in the volume of excavated rock. Discrepancies between the observed and predicted radiated energies indicated that strain energy in selected zones in the rock mass was either scattered if the prediction was overestimated, or accumulated if underestimated. Moreover, the study showed that elastic deformation in one zone can lead to inelastic deformation in the same zone.

1. Introduction

Underground excavation results in failure processes, e.g. deformations, taking place in the rock mass surrounding mined longwall panels. These processes are reflected in seismicity characteristics and seismic source mechanisms which can be used to reveal the history of rock mass mechanics during the excavation. Moreover, such knowledge is useful for understanding the phenomenon of rock mass destruction and can be used to reduce seismic hazard in mines. Seismicity in mines is usually caused by the presence of unfavourable geological conditions such as the depth of exploitation, hard and rigid rocks forming roof-rocks and floor-rocks, as well as footwall or/and hangingwall strata, faults, and others mining layouts [1]. Additionally, mining conditions also strongly affect the seismicity level which is caused by the presence of gobs, systems of roof control, safety pillars, and edges of old mined longwall panels. They disturb the local stress regime just as natural discontinuities present in the rock mass do [2,3].

Spatiotemporal seismicity rate anomalies are generally reported as the most frequent intermediate-term precursory phenomenon of seismic hazard in time-scales varying from a few days to several years [4]. Recent studies focused on two approaches i.e. parametric and non-parametric approaches. The first approach is based on the use of the well-established Gutenberg-Richter law which was applied in many pieces of research on seismic hazard in mines [1,4–7]. In the second approach, the non-parametric hazard assessment approach is evaluated under certain conditions [8,9]. Seismicity in mines can lead to dangerous damages in operating longwalls, openings, galleries, etc., resulting in rockburst [10]. The mined total volume of rock associated with hard coal exploitation corresponds to an increase in the level of seismicity, thus this relationship can be used to evaluate an algorithm estimating seismic hazard which varies overtime [11,12].

To deal with the seismic hazard in mines, prevention techniques are applied during underground workings. One of those techniques is the usage of destress blasting in order to minimize the strain energy in a rock mass. Quantitative methods, attempting to assess the effectiveness of the blasting, were introduced by Konicek et al. [13,14], Wojtecki and Konicek [15], Wojtecki et al. [3,16,17], and Konicek and Schreiber [18]. The assessment of the effectiveness

* Corresponding author.
E-mail address: maciej.mendecki@us.edu.pl (M.J. Mendecki).

https://doi.org/10.1016/j.ijmst.2020.12.001
2095-2686/

is based on the analysis of mining tremors' focal mechanisms occurring after the blasts, assuming that the focal mechanism parameters carry the information about local stress and strain energy conditions. The focal information was obtained by calculation of the full seismic moment tensor (SMT) and/or spectral source parameters. SMT defines the force system occurring in the seismic point source considering a linear combination of force couples and it describes the seismic source in the focus entirely and completely [19]. The spectral source parameters are estimated from the simple well-known seismic source model presented by Brune [20] and developed by Madariaga [21], who verified and changed the concept of the source radius. Both models describe the source as a circle with a specific radius, size (scalar seismic moment and magnitude), displacement, energy release, static stress drop, and apparent stress. These spectral parameters are obtained from a fitted model of the displacement spectra (P-waves and S-waves) as a function of frequency. The displacement spectra are characterized by two main parameters i.e. the corner frequency and spectral level which correspond to focus size and character of physical processes occurring during the rapture [11,22].

Spectral source parameters can be used to calculate the source and apparent volumes which correspond to coseismic inelastic deformation that radiates the seismic waves. Mendecki [22] noted that these two parameters have a predisposition to be precursors that can be used in short- and medium-term predictions and can be easily calculated from ratios of spectral source parameters, i.e. scalar seismic moment, stress drop, and apparent stress, respectively. The elastic (reversible) deformation is defined as a process during which no new microcracks are originated while all existing microcracks propagate in the rock mass without growing in size [22]. The potential energy accumulated during elastic dislocation may be discharged or it may be released gradually or abruptly during the processes of inelastic deformation. The inelastic (irreversible) deformation of brittle-like rock is mainly due to fracturing and frictional sliding called cataclastic flow resulting in emitted seismic waves. Their amplitude and frequency depend, in general, on the toughness and stress state in the rock mass, the focus size, and on the fracturing process rate at which the rock mass is damaged. Generally, a mining tremor resulting from disequilibrium in the flow of rock and, as whirls in the fluid flow, can be demonstrated as a consistent diffusing structure which contains newly-created useful data. Formation of such data (hidden information) must be combined with extended diffusing rates, i.e. an increase in dislocation rate at the seismic source produces more seismic radiation [22].

The purpose of this article is to investigate the focal mechanisms and source parameters of underground mining tremors within coal seam No. 507, in the Ruda hard coal mine in the Upper Silesian Coal Basin, Poland (Fig. 1a). The studied longwall panel in coal seam No. 507 was designed to maximally utilize the effect of stress relaxation caused by the presence of the earlier excavated coal seams deposited above. The study is based on parametric statistical analyses of 1016 selected seismic events recorded and located by the mine seismic network, with a local magnitude (M_L) higher than or equal to 0.6. Next, 18 relatively strong tremors were chosen for focal parameters analysis. A cutoff level was assumed as M_L = 1.5 (i.e. seismic energy 5 $\times$ 10^4 J). This limit was taken because of two reasons: (1) the acquisition of a representative group of relatively strong event representing general rock mass behaviour during excavation, and (2) the quality of the seismic records. The purpose of the 18-event analysis was to reconstruct the probable course of destruction processes in the rock mass and in the area of the longwall panel and to indicate in which zones the strain energy was accumulated or scattered as well as where the process of seismic deformation was mainly elastic or inelastic. This history of stress-strain changes in the rock mass was revealed using SMT, spectral source parameters, and energy-volume relationship.

2. Site characterization, longwall panel seismicity, and seismic hazard

Coal seam "No. 507's" longwall panel was mined over a period of nine months, in the eastern part of the selected hard coal mine, located in the Main Anticline, the Upper Silesian Coal Basin, Poland (Fig. 1a) [23]. Longwall mining was designed in a traversing system with roof-rock caving. The studied longwall panel was designed to utilize the maximum effect of stress relaxation through earlier exploitation in coal seams Nos. 502 and 504, and in a small range in coal seam No. 506. Below the longwall panel, mining was not carried out. Whether the three coal seams, over coal seam No. 507 (Fig. 1d), had a direct impact on the studied longwall mining was investigated. The three exploitations were carried out in the following coal seams: (1) seam No. 502, deposited approximately 124 m above, which was in total mined over the entire longwall panel (12 and 21 to 22 years before); (2) seam No. 504, deposited approximately 61–70 m above, which was almost entirely mined over the longwall panel, except for two small fragments in the southern and the eastern part (10 and 13 years before); and (3) seam No. 506, deposited approximately 27 m above, which was excavated only over the northern part of longwall panel (36 to 37 years before). Therefore, at the beginning, the mining was carried below the edge in seam No. 506.

The coal seams were interbedded with thick layers of sandstones, shales, and sandy shales (Fig. 1c). The layer strike had the direction from ESE-WNW to ENE-WSW. The studied coal seam was characterized by two main orientations of crack systems (strike, dip, dip direction): 16°/50°–85°/E and 85°/70°–90°/S. In the roof-rocks of coal seam No. 507, the crack systems changed directions 97°/55°–75°/S and 193°/50°–65°/W. Several local faults were detected in the study area during the mining operations. Their strike directions were in accordance with the crack systems direction (ESE-WNW to ENE-WSW) with deviation to the SW-NE direction. The slips of those faults ranged from 0.8 to 1.8 m and their dips ranged from 40° to 80° in the SE direction. During the drilling of longwall galleries, rockburst prevention was performed, mainly in the form of destress blasts, which produced mining tremors characterised by seismic energies ranging from 10^2 to 10^3 J. Preliminary rockburst hazard assessment qualified this longwall for excavations as slightly threatened by rockbursts.

The mine seismic network consisted 18 seismic stations (15 underground and 3 surface station, Fig. 1b), and enabled to monitor the seismic activity during longwall mining of coal seam No. 507. Most of the seismic sensors were located to the south from the longwall panels in coal seam No. 507. Hypocentres and seismic energies of mine tremors were estimated using the ARAMIS seismic observation system installed in underground excavations and provided by EMAG Company, Poland. The energy of strong tremors (i.e. with the seismic energy higher than or equal to 1 $\times$ 10^5 J, what corresponds to the local magnitude M_L = 1.68) was verified by the Upper Silesian Regional Seismological Network which belongs to the Central Mining Institute, Poland. The surface seismic stations belonged to the AMAX-GSI system, produced by Central Mining Institute, Poland.

The level of seismicity in the studied longwall panel was described by the frequency-magnitude distribution for local magnitudes for a total of 1016 selected events, the Gutenberg-Richter distribution and the comparison of empirical and calculated cumulative probability (Fig. 2a–c). The seismic hazard analysis during mining of the studied panel was calculated based on the magnitude distribution [5].

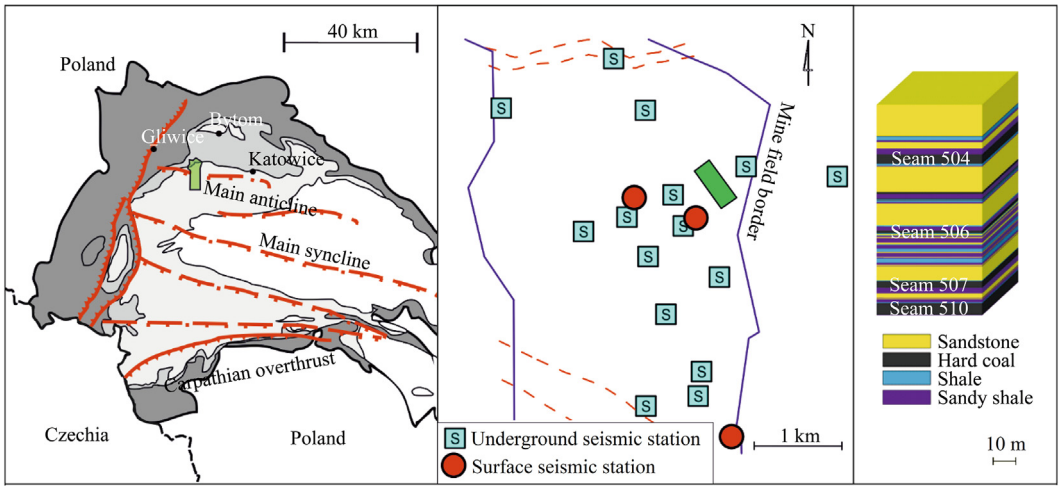

(a) General map of the Upper Silesian Coal Basin, green area—mine field

(b) Sketch of mine-field border with surface and underground seismic stations and main fault zones, the studied longwall was marked as green rectangle

(c) Generalised geology profile in the area of the selected longwall panel

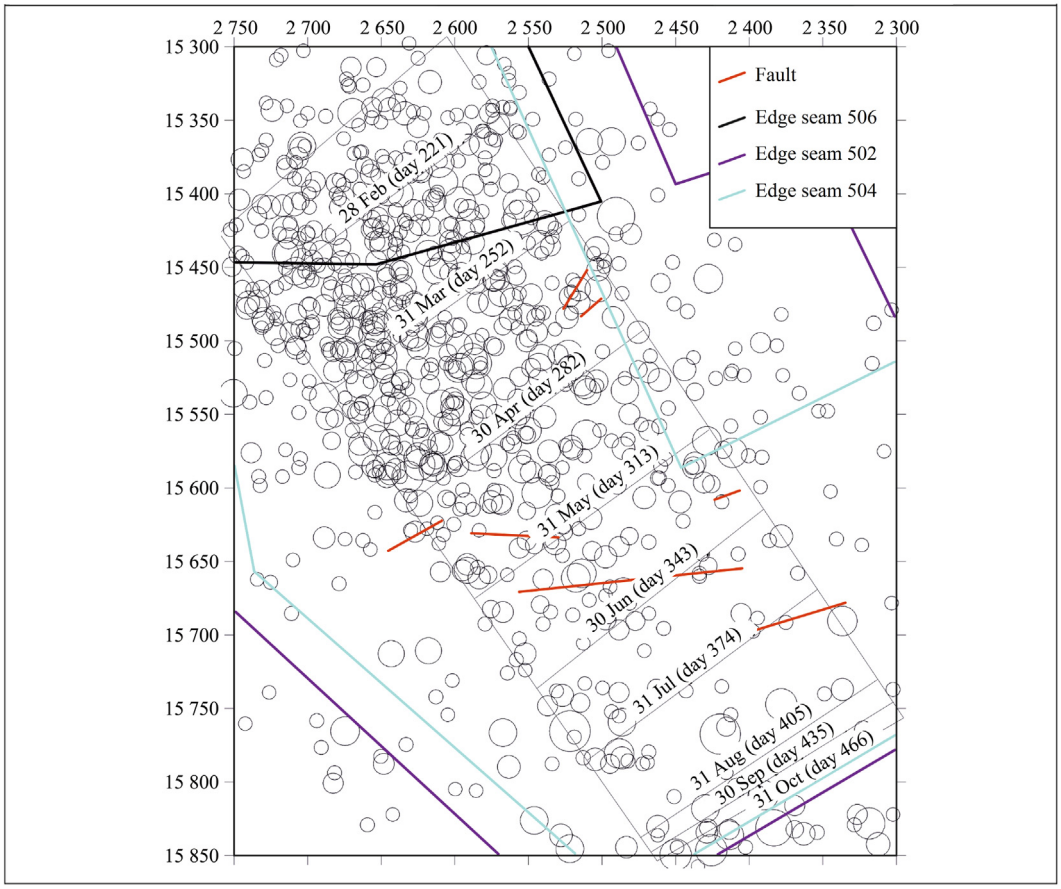

(d) Seam map with seismic event location and mining edges, circle size corresponds to local magnitude.

Fig. 1. Site characterization.

$$F(M_L) = 1 - \exp(-\beta(M_L - M_{min})) \quad (1)$$

where M_L is the considered local magnitude (for the Upper Silesian Coal Basin) from the catalogue; M_{min} the minimum magnitude; $F(M_L)$ the cumulative magnitude distribution; and β the parameter expressed as follows.

$$\beta = 1/(M_L - M_{min}) = b/\log_{10}(e) \quad (2)$$

where b is the Gutenberg-Richer parameter. During this study, it was assumed that the minimum magnitude corresponds to the magnitude with the largest occurrence frequency of seismic events in the low-energy range (Fig. 2a). The analysis of the seismic catalogue from the studied longwall panel indicated that the minimum magnitude is 0.6. The Gutenberg-Richter distribution for the studied catalogue was presented in Fig. 2b. The b-value was relatively

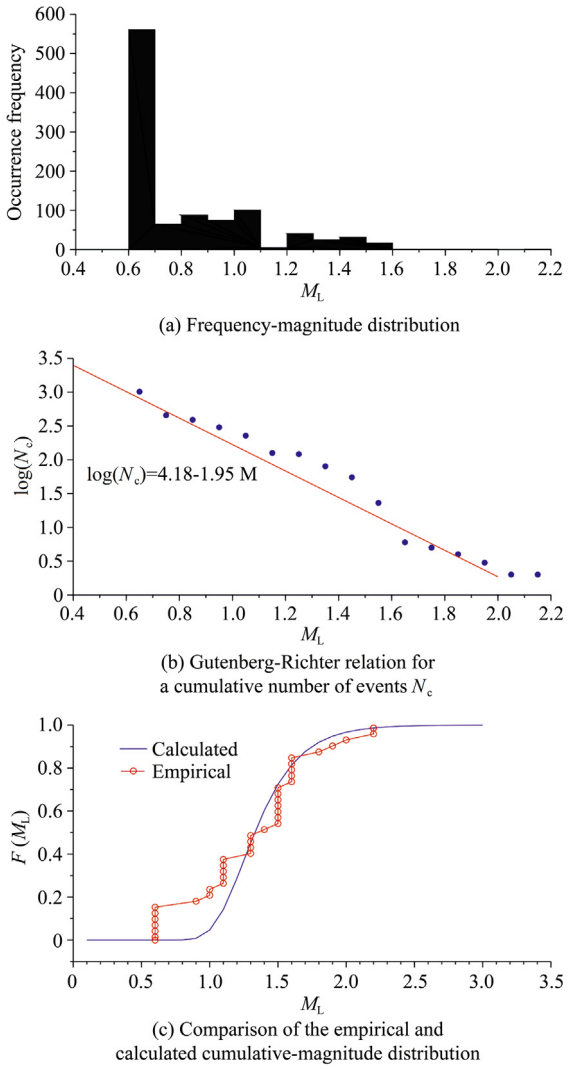

(a) Frequency-magnitude distribution

(b) Gutenberg-Richter relation for a cumulative number of events N_c

(c) Comparison of the empirical and calculated cumulative-magnitude distribution

Fig. 2. Seismicity characterization.

high and reached 1.95 which corresponds to a high level of low-energy seismicity in the study area.

The maximum probability distribution was calculated based on the known magnitude/energy distribution and the assumption that the event frequency distribution in a short or long period is the Poisson distribution. Thus, the cumulative probability distribution function of the maximum energy event, $G(M_L^{max})$, can be expressed as follows [1,5].

$$G(M_L^{max}) = \frac{\exp(-\lambda\Delta t(1 - F(M_L))) - \exp(-\lambda\Delta t)}{1 - \exp(-\lambda\Delta t)} \quad (3)$$

where λ is the event frequency overtime (the Poisson factor); and Δt the time interval width (10 days). The empirical cumulative distribution function, G_{emp}, was estimated based on Eq. (4) [5].

$$G_{emp}(M_L^{max}) = (i - 0.5)/w \quad (4)$$

where i is the number of maximum energy events in the interval; and w the interval. The estimated cumulative magnitude distribution $F(M_L)$ enabled the calculation of the cumulative probability distribution function of the maximum magnitude for the entire seismic catalogue (Fig. 2c) and comparion with the empirical distribution.

The visual inspection provided a satisfactory comparison of both distributions and convinced us to use this data to estimate the probability of the occurrence of an event with a certain magnitude/energy or larger during the selected time interval. This calculation required two assumptions, the first being that the analysed process is stationary for a short time interval, thus 10-day intervals were chosen and the second being that the intervals contain a sufficient number of events. This second condition is difficult to fulfil, however, in the studied case, the minimum number of event in the 10-day intervals reached 5, the maximum was 114 and the average was 33.7 per interval. The probability of exceeding certain energy, $R(E,t)$, can be estimated as follows [5].

$$R(E,t) = (1 - \exp(-\lambda(t)\Delta t))(1 - F(E,t)) \quad (5)$$

where $F(E,t)$ is the Pareto's distribution for energy [5] which produced similar distribution to magnitude distribution (Fig. 2c). The Poisson factor and the energy distribution are varied with time. The results of the exceedance probability calculated for the energy of 1×10^5 J per 10-day period are shown in Fig. 3. The start date corresponds to the occurrence of the first weak event in this area and is associated with preparation works. This probability was compared with the monthly excavated volume of rocks and the longwall face advances (Fig. 3). The comparison indicated that the excavated volume of rock correlates with an increase of seismic hazard. Two maxima can be noticed when the longwall face was close to the edges of overlying coal seams (No. 504 in the eastern part and Nos. 504 and 502 in the southern part of longwall panel).

3. Methods and results

3.1. Source mechanisms and source parameters of $M_L \geq 1.5$ events

The analysis of foci was based on two independent studies: the solution of the full SMT and the estimation of spectral source parameters. The analyses required high-quality data, i.e. first P- and S-wave arrivals are clearly visible. 18 events with local magnitudes of $M_L \geq 1.5$ from 1016 events were chosen. It was assumed that the event population, their distribution, and their focal mechanisms are the data set which can represent the general behaviour of rock mechanics and changes of stress regime in the roof-rocks for the analysed longwall.

The SMT solutions were calculated in the FOCI software [24] based on the seismograms recorded by the mine seismic network [24]. The FOCI software is the stand-alone Windows GUI application that allows to perform both the SMT inversion and source parameters calculation using waveform data and it was created by Grzegorz Kwiatek. The application is optimized for local-to-regional applications and seismic networks. The focal mechanism calculations used the inversion of the first P-wave amplitudes using the L1 norm and the full SMT solution was carried out due to the possible participation of various processes in induced tremor

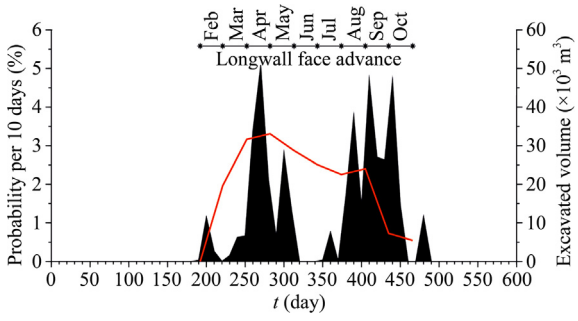

Fig. 3. Probability of the occurrence of an event with the energy of $>10^5$ J per 10-day interval (black areas) and the excavated volume of coal per monthly longwall face advance (red line).

sources (shear, explosion, implosion, uniaxial compression or stretching). The principles of SMT calculation were presented by Aki and Richards [19] and this solution is widely applied in global and mining seismology. The exact location of the hypocenter was very important for the correct determination of the focal mechanisms. The mining observation system provides the event coordinates *X*, *Y*, and *Z* in the Sucha Góra Local Geodetic System which is standardly used in mines in the Upper Silesian Coal Basin. The location of the tremor foci was obtained using the P-wave first arrivals method. The horizontal location error ranged from 25 to 38 m, while the vertical coordinate was corrected and refined using FOCI software. The best focal depth was assumed if the solution quality factor was the highest and errors of the determined SMT components were the smallest. The final results of the full SMT solution contained: percentages of SMT components in %, type of mechanism, and parameters of nodal planes A and B (Table 1). Concerning strong events, these results are in accordance with the paper of Wojtecki et al. [25] in which the influence of the mining edges of overlying seams was analysed. This study was based on the full SMT solution of seven strong events. Five of them were also used in this study.

Spectral source parameters characterizing the focal mechanism were calculated on the basis of Brune's model [20] which was implemented using the FOCI software [24]. Spectral parameters were estimated using both the seismic wave velocity records transformed to frequency domain $V(f)$ and the calculated displacement spectrum $D(f)$. Next, the $V(f)$ and $D(f)$ spectra are integrated into $J(f)$ and $K(f)$ functions, respectively, known as Snoke's functions [24] and they can be expressed as

$$\begin{cases} J = 2\int_0^\infty V^2(f)df \\ K = 2\int_0^\infty D^2(f)df \end{cases} \tag{6}$$

In practice, both power spectra are calculated for finite frequency limits (lower and upper). The lower limit is a reciprocal of the event duration time and the upper limit is defined as Nyquist frequency. The $J(f)$ and $K(f)$ functions enabled the independent calculation of the spectral level Ω_0 and corner frequency f_0, and then the rest of the parameters according to Brune's model: scalar seismic moment M_0, moment magnitude M_w, source radius r_0, seismic energy E_0, stress drop $\Delta\sigma$, and apparent stress σ_a [16,22]. The results of the obtained spectral source parameters are presented in Table 2.

The reverse source mechanism was observed in 12 events in which most of the full SMT solutions showed a relatively large percentage of double-couple (DC) component, i.e. from 29.6% to 94%, as well as five of them also possessing a relatively large percentage of isotropic (ISO) component (>20%). The location of these events are usually close to the longwall face and the nodal plane strikes, generally, covered the longwall face (8 cases) and seam edge orientations (4 cases), which led to the assumption that those events were induced or triggered by the mining operation. A fracturing of sandstones deposited in the roof of coal seams Nos. 507, 506, and 504 (Fig. 1c), and over the longwall panel was the most probable factor responsible for the occurrence of those seismic events. These criteria are in accordance with the widely discussed discrimination procedure of tectonic and anthropogenic seismicity in Poland [26].

In the case of the reverse source mechanisms, the average shearing component of SMT was large and exceeded 58%, which can be correlated with the fracturing of sandstones deposited in the roof. One event, No. 8, was characterised by almost pure shear with a DC component of 94% which probably represents a triggered mechanism. The percentage share of the ISO component, i.e. explosion, equalled on average approximately 20.0%, and of the compensated linear vector dipole (CLVD) component, i.e. compensated

Table 1
Result of the full SMT solution of 18 analysed seismic events.

No.	Date	Time	Sucha Góra coordinate			E ($\times 10^4$ J)	M_L	Nodal plane A			Nodal plane B			Component			Mechanism type
			X (m)	Y (m)	Z (m)			Strike (°)	Dip (°)	Rake (°)	Strike (°)	Dip (°)	Rake (°)	ISO (%)	CLVD (%)	DC (%)	
1	2017-03-17	21:53:38	15540	2690	−410	5.00	1.53	134.3	56.2	95.5	304.5	34.2	81.9	35.3	15.5	49.1	Reverse
2	2017-03-30	04:43:11	15410	2560	−550	5.00	1.53	159	65.7	−43.3	270.2	51.3	−148.1	−43.5	−5.8	50.8	Normal
3	2017-03-31	16:01:29	15369	2582	−580	8.00	1.63	358.1	65.8	29.6	255	6.2	152.6	−27.7	−13.3	58.9	Normal
4	2017-04-03	17:29:52	15401	2647	−580	6.00	1.57	234.1	57.4	100.8	34.7	34.2	73.7	27.6	42.8	29.6	Reverse
5	2017-04-03	21:12:37	15418	2494	−450	40.00	2.00	234.8	68.0	90.1	56.6	22.0	72.9	25.2	28.0	46.8	Reverse
6	2017-04-08	01:28:21	15409	2599	−500	8.00	1.63	234.2	59.1	104.3	27.8	33.7	67.6	21.9	29.2	48.9	Reverse
7	2017-04-13	09:06:54	15419	2558	−510	20.00	1.84	235.8	58.5	106.4	26.4	35.1	65.3	24.3	23.3	52.5	Reverse
8	2017-04-13	23:02:30	15514	2591	−540	8.00	1.63	237.8	67.3	117.1	4.7	34.8	42.5	5.3	0.7	94.0	Reverse
9	2017-04-14	10:42:39	15511	2659	−500	7.00	1.60	235.5	61.8	100.3	34.5	29.9	71.5	25.3	31.3	43.4	Reverse
10	2017-04-15	01:52:18	15517	2588	−400	7.00	1.60	19.7	84.9	107.8	125.3	18.5	16.4	8.6	11.5	79.9	Reverse
11	2017-04-18	02:35:43	15604	2547	−400	6.00	1.57	25.2	83.3	106.6	136.5	17.8	22.3	11.2	12.4	76.4	Reverse
12	2017-04-18	17:26:19	15443	2713	−410	7.00	1.60	310.6	52.5	−85.8	123.7	37.7	−95.4	−37	−30.4	32.6	Normal
13	2017-04-19	03:56:02	15585	2626	−410	7.00	1.60	314.9	52.7	98.6	121	38.2	79	34.5	21.5	44.0	Reverse
14	2017-04-20	01:41:03	15593	2634	−400	8.00	1.63	12.6	79.3	108.8	131.2	21.5	30.3	14.1	15.4	70.5	Reverse
15	2017-07-13	06:27:39	15886	2549	−580	8.00	1.63	344.8	63.5	−62.6	115.5	37.4	−132.7	−31	−11.3	57.7	Normal
16	2017-08-01	22:32:13	15829	2388	−580	30.00	1.94	257.3	72.4	96.5	56.6	18.7	70.4	15.6	21.9	62.5	Reverse
17	2017-08-21	18:59:03	15766	2424	−540	90.00	2.19	342.6	55.2	−52.7	109.5	49.2	−131.1	−32.5	−5.7	61.8	Normal
18	2017-09-12	17:40:19	15764	2525	−510	100.00	2.21	338.3	58.6	−62.7	113.4	40.7	−127.0	−34.1	0.2	65.7	Normal

Table 2
Spectral source parameters of 18 analysed seismic events.

No.	Date	Time	Sucha Góra coordinate			J ($\times 10^{-10}$)	K ($\times 10^{-13}$)	Ω_0 ($\times 10^{-8}$)	M_0 ($\times 10^{11}$ Nm)	f_0 (Hz)	M_w	r_0 (m)	E_0 ($\times 10^4$ J)	$\Delta\sigma$ ($\times 10^5$ Pa)	σ_a ($\times 10^2$ Pa)
			X (m)	Y (m)	Z (m)										
1	2017-03-17	21:53:38	15540	2690	−410	11.80	2.23	7.8	7.1	9.90	1.81	99.2	16.6	8.59	32.2
2	2017-03-30	04:43:11	15410	2560	−550	8.60	4.95	14.5	10.8	8.55	1.92	135.4	18.4	11.60	43.3
3	2017-03-31	16:01:29	15369	2582	−580	5.95	8.73	27.8	34.3	4.22	2.24	217.2	17.6	1.77	6.6
4	2017-04-03	17:29:52	15401	2647	−580	7.84	23.10	36.8	43.2	6.76	2.14	178.6	26.5	5.44	20.4
5	2017-04-03	21:12:37	15418	2494	−460	11.10	41.60	51.9	61.8	5.86	2.28	189.9	37.1	5.22	19.6
6	2017-04-08	01:28:21	15409	2599	−500	5.25	4.80	16.3	18.9	7.00	2.03	161.7	13.8	3.54	13.3
7	2017-04-13	09:06:54	15419	2558	−500	4.16	8.97	26.0	30.5	6.03	2.17	178.0	14.6	3.90	14.6
8	2017-04-13	23:02:30	15514	2591	−540	1.35	1.45	11.1	12.7	6.22	1.99	169.8	3.5	2.62	9.8
9	2017-04-14	10:42:39	15511	2659	−500	1.77	2.58	16.1	19.2	4.49	2.12	193.1	5.1	1.26	4.7
10	2017-04-15	01:52:18	15517	2588	−400	2.01	3.00	17.0	20.7	4.65	2.14	188.1	6.1	1.44	5.4
11	2017-04-18	02:35:43	15604	2547	−400	2.46	1.86	11.5	12.9	5.64	1.99	163.0	5.4	1.76	6.6
12	2017-04-18	17:26:19	15443	2713	−410	18.40	3.45	97.3	11.9	9.65	1.95	142.8	52.0	15.70	58.7
13	2017-04-19	03:56:02	15585	2626	−410	3.68	1.75	11.5	13.2	6.28	2.03	162.1	8.7	3.33	12.5
14	2017-04-20	01:41:03	15593	2634	−400	4.93	3.52	17.8	21.4	6.50	2.14	193.0	11.8	5.12	19.2
15	2017-07-13	06:27:39	15886	2549	−580	5.22	5.85	27.0	31.2	4.99	2.22	223.3	10.8	1.85	6.9
16	2017-08-01	22:32:13	15829	2388	−510	4.90	7.69	26.1	34.4	5.63	2.20	181.2	14.0	2.74	10.3
17	2017-08-21	18:59:03	15766	2424	−540	13.30	8.52	23.7	28.1	6.09	2.15	174.8	26.2	5.63	21.1
18	2017-09-12	17:40:19	15764	2525	−510	30.40	95.30	94.6	133.0	4.43	2.51	230.8	126.0	4.49	16.8

linear vector dipole, equalled 21.1%. Tremors correlated with the near-seam processes of destruction are usually characterized by a small shearing component in the full SMT solution and very high non-DC components with the ISO component from 20% to 50%. In the foci of the analysed tremors, the percentage share of the DC component can be classified as high, which suggests that destruction processes were correlated with the fracturing of overlaying sandstones. However, the relatively small magnitudes of these rest events did not suggest that the origin could be triggered. Six normal fault focal mechanisms also showed the relatively large values of components: DC (>30%, mean 54.5%) and ISO (<−27%, mean −34.3%). The negative isotropic component indicates that in the focal mechanism an implosion also occurred. The obtained "beach balls" representing seismic mechanisms are shown in Fig. 4.

To summarise, the studied events indicate roof-rock cracking with inelastic deformations caused by mining excavation which followed the longwall face advance.

3.2. Source and apparent volumes

A mining tremor can be considered as a sudden inelastic deformation within a given volume of rock that radiates detectable seismic waves. In this case, the average stress drop obtained as one of the spectral source parameters can be explained as a spatial density of the seismic moment M_0 and the source volume V which can be presented as [22]

$$V = M_0/\Delta\sigma \tag{7}$$

In Eq. (7) the scalar seismic moment corresponds to the moment tensor, thereby the moments of force couples acting in the source. Therefore, the source volume can be considered to be a system of couples located at the centre of this region with the largest inelastic shear strain drop resulting in deformation. The volume of rock associated with the coseismic inelastic dislocation changes from a fraction of m^3 for cracks of approximately 1 m in length to a fraction of km^3 for large seismic events with source dimension of a few hundred meters. For mine tremors, the average strain change within the source volume varies from 10^{-4} to 10^{-2} [22].

Mining tremors that occur near to the underground openings and/or in complex geological structures very often demonstrate a volumetric character, with many zones of long-lasting deformation and complicated geometry associated with a local volume variation. Therefore, the apparent volume for a seismic event (V_A) corresponds to the rock volume with coseismic irreversible strain with accuracy in the order of magnitude of apparent stress divided by stiffness. It can be defined as [22]

$$V_A = M_0/2\sigma_a \tag{8}$$

Eq. (8) shows that apparent volume depends on the seismic moment and apparent stress, and thus on radiated seismic energy. The aforementioned relations lead to the assumption that both apparent volume and source volume acquires sensitivity to the inelastic coseismic deformation from its two-dimensional description of the seismic source, namely, by seismic moment and seismic energy or by seismic moment and stress drop [22].

The apparent volumes for the selected seismic events were calculated based on spectral source parameter results (Table 3). The apparent volumes varied from 1.014×10^8 to 39.580×10^8 m^3. The location of these events and the corresponding values of apparent volume were used to map the spatial distribution of the volumes (Fig. 4). The mapping was carried out by the application of the inverse distance to a power technique. This gridding method is one of the more common methods used in natural sciences in which the value assigned to a grid node is a weighted average of either all of the data points or a number of directionally distributed

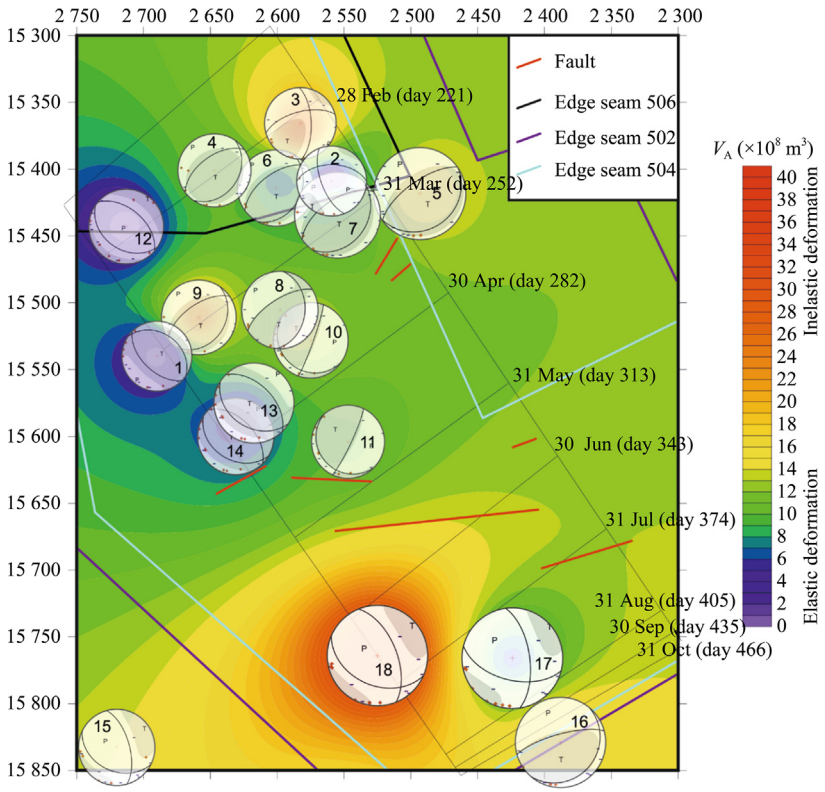

Fig. 4. Distribution of apparent volume with the full SMT solutions of the 18 studied seismic events, dates and day numbers indicate the longwall face advances.

neighbours. The values of each data point, in this case, were weighted according to the inverse of its distance from the grid node, taken to the power of 2. Moreover, this gridding method produces a smooth and continuous grid and does not exaggerate its extrapolations beyond the given data points [27,28]. The results of the apparent volume mapping showed that the first part of the studied longwall panel was characterised by low values of the apparent volume, especially along the west edge of the panel. It suggests that this area was associated with dominating elastic deformations. Next, the advancing exploitation caused the occurrence of larger apparent volumes and the largest values were observed at the end of the studied longwall panel (Fig. 4).

3.3. Relationship between released energy and the excavated volume of rocks

Time-dependent seismic hazard assessment in mines can be associated with a statistical relationship between sum of seismic energy and the excavated volume of rocks. Usually, the energy-volume relation can be simply expressed as a power law [5,11]. In this case, a similar relationship is proposed which is exponential, as follows.

$$\sum_{j=1}^{n} E_j = c_1 \cdot \exp(c_1 V) \tag{9}$$

where E_j is j-th event energy in a time inverval; $j = 1, 2, \ldots, n$; n the number of all energies summed in a time interval; V the excavated volume of rock in a specific time interval; and c_1 and c_2 the constants. The time interval was assumed as monthly longwall face advance. If constants c_1 and c_2 are estimated and the excavated volumes are known, it is possible to predict the expected energy release per time interval. The comparison of the observed energy, radiated from the rock mass, with the predicted one can provide information outlining whether the strain energy was concentrated or scattered due to the mining and geological conditions. It was assumed that the accumulation of strain energy in the rock mass corresponds to the situation that the predicted seismic energy release is underestimated, thus the observed sum of energy per month released is higher than the predicted one. It indicates that in the rock mass additional strain energy originated from disturbances in the stress regime and from stress transfers caused by the previous mining operation was accumulated. The scattering of strain energy was assumed in the case of the overestimation of the predicted energy release. The scattering of energy corresponds to the situation that the present mining operations generated strain energy in the rock mass, but it was transferred and distributed to weaknesses or dislocation located in the surroundings of the longwall panel, for instance, other mining edges or gobs can be treated as those weaknesses. Thus it was assumed that exponential seismic energy release relation corresponds to balanced, regular energy release due to longwall mining and the observed deviations from the "average" conditions are related to accumulation or scattering of energy (Fig. 5a).

The energy-volume relation was found using rigid regression with the rigid parameter of 0.5 [29]. The results showed that c_1 = 100.3 and c_2 = 0.00015. The estimated relation (Eq. (9)) with the observed and predicted values of the energy radiated is presented in Fig. 5a. The modelled curve showed two areas, one over the line was interpreted as an area of strain energy accumulation and the second, below the model, as an area of scattered energy. If the observed values of released energy were located in a specific area, then this provided information about strain energy distribution during exploitation. In cases when the observed and predicted distribution were almost equal, then it was assumed as a balanced state, i.e. induced strain energy was regularly radiated from rock masses at the same time interval. Additionally, the observed and predicted values of energy release were plotted against time

Table 3
Values of the apparent volume for the selected seismic events.

No.	Date	Time	Sucha Góra coordinate			V_A ($\times 10^8$ m^3)
			X (m)	Y (m)	Z (m)	
1	2017-03-17	21:53:38	15540	2690	−410	1.098
2	2017-03-30	04:43:11	15410	2560	−550	1.247
3	2017-03-31	16:01:29	15369	2582	−580	25.870
4	2017-04-03	17:29:52	15401	2647	−580	10.590
5	2017-04-03	21:12:37	15418	2494	−460	15.760
6	2017-04-08	01:28:21	15409	2599	−500	7.105
7	2017-04-13	09:06:54	15419	2558	−500	10.440
8	2017-04-13	23:02:30	15514	2591	−540	6.466
9	2017-04-14	10:42:39	15511	2659	−500	20.380
10	2017-04-15	01:52:18	15517	2588	−400	19.240
11	2017-04-18	02:35:43	15604	2547	−400	9.802
12	2017-04-18	17:26:19	15443	2713	−410	1.014
13	2017-04-19	03:56:02	15585	2626	−410	5.280
14	2017-04-20	01:41:03	15593	2634	−400	5.573
15	2017-07-13	06:27:39	15886	2549	−580	15.000
16	2017-08-01	22:32:13	15829	2388	−510	16.700
17	2017-08-21	18:59:03	15766	2424	−540	6.659
18	2017-09-12	17:40:19	15764	2525	−510	39.580

(Fig. 5b). This showed the periods when strain energy was scattered or accumulated in the rock mass. Visual inspection of Fig. 5b indicated that at the beginning of the longwall panel (days 200–280) the strain energy was scattered, in other words, less seismic energy was radiated from the rock mass than could be expected from the amount of the excavated volume of rocks. The longwall was in the starting phase, and there were problems with the roof falling behind the longwall face [17]. The process of destruction probably only concerned the rocks deposited in the direct roof. The advancing exploitation reached the zone where the previously concentrated strain energy started releasing seismic energies which are higher than those expected from the model (days 250–310).

The rock mass in this area was affected by the local faulting system and the edge of coal seam No. 504 which was over the eastern part of the longwall panel (Fig. 4). However, coal seam No. 504 was extracted in this area about 13 years earlier, so the actual destress effect was smaller. Additionally, the processes of destruction embraced the layers of sandstones deposited at greater distances from coal seam No. 507 (over coal seam No. 506 and probably over coal seam No. 504).

Next, according to the advancing exploitation, the mining conditions changed. Coal seam No. 504 was extracted 10 years earlier, and the destress effect was greater than that in the previous phase, which corresponded to the scattering of strain energy (days 310–380). However, systems of local faulting were present in this part of the longwall panel (Fig. 4). The seismic energy radiated from the rock mass was once again smaller than expected from the energy-volume relation. Finally, the longwall face approached the end of the designed panel size and reached the zone where two edges (seams Nos. 502 and 504) were located (days 380–480). The lower longwall face advance (Fig. 3) in this phase should have also caused strain energy scattering in the rock mass. However, the opposite effect was observed. The smaller excavated volume corresponded to a higher level of seismicity and large seismic energy release. The probable causes of this effect are discussed below.

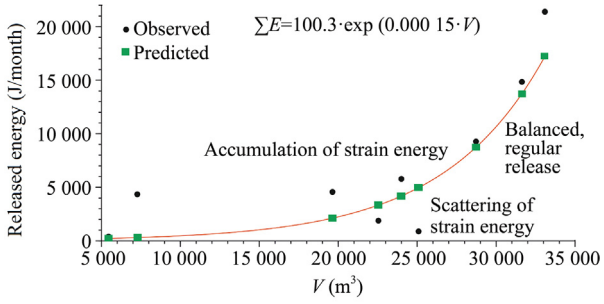

(a) The model of the relation between released energy and the excavated volume of rocks in comparison to observed values

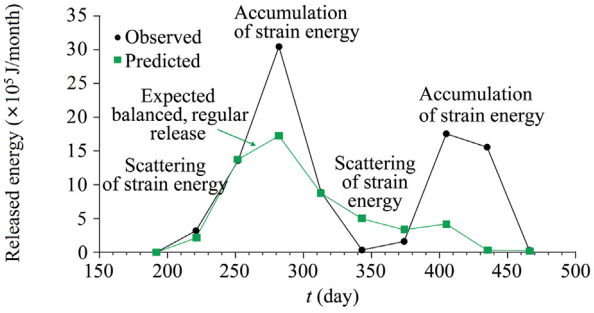

(b) Deviations of the observed energy release per month with the predicted/expected values vs. the time of exploitation

Fig. 5. Calculation results of the energy-volume relation.

4. Discussion

The applied methodology and obtained results enabled the observation of variations in the seismic hazard, excavated volume of rock, the strongest event mechanisms, apparent volume, inelastic and elastic deformations, and energy released during the mining operation. All of these findings can reveal the history of rock mechanic behaviour under the exploitation and changes in mining and geological conditions. This probable behaviour reflected the total deflection of the roof-rocks as a result of the longwall mining. It disturbed stress regime in this area resulting in a higher level of seismicity. The authors have focused on the link between the inelastic and elastic deformations in the roof-rock (based on the estimated seismic source parameters) with the scattered or concentrated strain energy in the rock mass in order to explain probable reasons for those variations.

4.1. Scattering and accumulation of strain energy

Analysis of the presented results changes over time and space which allowed three main cases of rock mechanic behaviour and two individual cases occurring during the mining operations to be distinguished. This comparison was based on the dependence between apparent volume and seismic energy release.

The first case related to the situation that the observed energy released is almost equal to what was predicted and the apparent volume is small, thus the elastic deformation was dominant in the rock mass. This case is observed for the event Nos. 1, 2, 4, 5, and 6. They were located at the beginning of the longwall panel, below the edge of coal seam No. 506. The predicted and observed released energy were similar which indicates that the excavation induced the strain energy and it was released and radiated from the roof-rocks almost simultaneously in a balanced way. This energy was not scattered to neighbouring discontinuities or other weaknesses in the rock mass. This lack of stress transfer at the beginning could correspond to insufficient deflection of the roof-rock due to the small volume of excavated rocks. The observed source mechanisms were mainly reversed and one was normal which could be related to the fracturing and deflection of the roof-rocks under the caving process.

The second case concerns the relationship that the observed energy released is larger than the predicted one (accumulated strain energy) and the apparent volume is large, thus the inelastic deformation dominated. This case is observed for the event Nos. 9, 10, 16, and 18. These events mechanisms were reversed aside from the last normal-like event. Event Nos. 9 and 10 occurred in the roof-rocks affected by caving, thus the deformation was inelastic. The total energy released in that period is larger than that expected from the model, therefore the concentrated strain energy was large and it was accumulated in the rock mass during exploitation. The lack of significant local disturbances (edges, faults) caused that these two events occurred as inelastic fracturing of the roof-rocks. The last two events (Nos. 16 and 18) occurred at the end of the panel excavation. The total energy released in this zone was much larger than that expected from the model. This is due to the strong disturbance in the stress regime in the terminal area of the panel which resulted from the total excavation of the panel and the significant deflection of the roof-rock. Although this area was affected by two edges of overlying coal seams, the stress regime and concentrated strain energy were large, thus the energy was not scattered effectively.

The third case assumed that the observed energy released is larger than the predicted one (concentrated strain energy) but the apparent volume is small, thus the elastic deformation dominated in the rock mass. This case concerns events Nos. 7, 8, 11, 12, 13, 14, and 17, and this data set is the largest, therefore the condition mentioned above can be treated as preferred for generating seismic events. These events represent elastic reverse or normal mechanisms occurring in the area of high concentration of strain energy which could not be scattered effectively due to the lack of neighbouring weaknesses or its level was so high that the edges or faults did not disperse it.

By analysing combinations of apparent stress and energy release, an additional condition can be distinguished. The observed energy released is smaller than the predicted one (scattered strain energy) and the apparent volume is small, thus the elastic deformation dominated and this case was observed for the event No. 15. This mining tremor occurred relatively far from the longwall panel and it could not be directly affected by the operations. Nevertheless, this event represents a specific situation where strain energy was scattered effectively, probably to edges of seam Nos. 502 and 504, and the mechanism was normal and elastic dislocation occurred. The second specific case is observed for the event No. 3 which is related to the condition that the observed energy released is almost equal to the predicted one and the apparent volume is large, thus the inelastic deformation dominated. The mechanism of this event was normal which indicated that, during the excavation in the area of this event location, significant inelastic displacement occurred causing local changes in the stress value.

The described combinations omitted one situation where the observed energy released is smaller than the one predicted and the apparent volume is large, thus the inelastic deformation dominated in the source. This suggests that this case is difficult to explain due to the principle of energy conservation in the rock mass. Inelastic deformations can appear if in the rock mass the high level of strain energy is observed and, during the rupture, this energy converts to seismic energy and inelastic deformations. However, a possible explanation can be obtained by analysing local rock mass heterogeneity.

4.2. Benioff strain release

Comparison of source and apparent volumes with focal mechanisms and the Benioff strain release provides a comprehensive study on rock mechanic behaviour during the total longwall panel excavation. The Benioff strain release in mines was introduced by Mendecki [22] and several cases were discussed in the paper of Mendecki et al. [30]. These studies enabled the approximation of the behaviour of the stress regime in the rock masses surrounding the studied longwall fields. Moreover, they discussed the study issue that could be used to better understand the processes occurring during underground exploitation. Therefore, the Benioff strain release analysis was also used in the presented study. The cumulative Benioff strain release, which is the root square of energy, was plotted in Fig. 6. This curve was divided by the intervals interpreted according to the scattering and concentration of strain energy criteria, especially those shown in Fig. 5b. The 18 events analysed were also marked in Fig. 6. The visual inspection indicated that several phases could be distinguished which correspond to changes in the Benioff strain release slopes and the occurrence of the analysed seismic events.

The first phase was characterised by the assumed equilibrium state at the very beginning of exploitations. The release in that period was very flat. Next, the first phase of the strain energy scattering corresponds to a quiescence-like sequence and the occurrence of any of the selected event $M_L \geq 1.5$ (days 200–230). This phase changed to more linear with a stable rate of Benioff strain release (days 230–260). During this phase, six previously analysed seismic events occurred which can be explained as the balanced released of

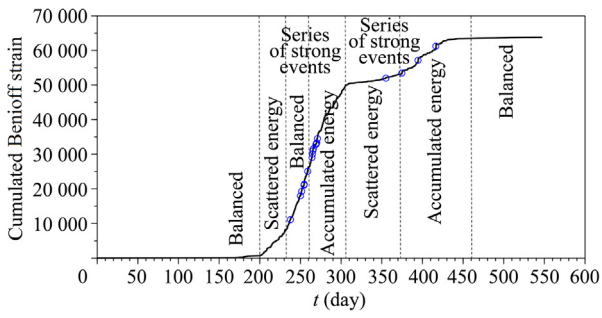

Fig. 6. Benioff plot. Blue circles denote the analysed 18 events.

seismic energy after the accumulation of strain energy due to the excavation advance. The roof-rocks and the panel surroundings were affected by different variations in stress regimes and stress transfer which change the Benioff strain release characteristics to quiescence-like type (more gentle slope between days 260–300). The time interval from days 250–300 was also characterised by the high level of seismic hazard (Fig. 3). However, the strongest events were concentrated only in the first part of this phase and then, on day No. 280, the extracted volume of rocks and seismicity decreased which was reflected in the quiescence-like behaviour of the Benioff strain release. The distribution of the strain energy also changed and it was dispersed in the rock mass. The next flat phase of Benioff strain release started on the day No. 310. The longwall panel was operating in the rock mass effectively destressed by the extraction of coal seam No. 504, about 10 years earlier. New fracturing in the roof-rocks occurred and the longwall face advance was approaching the zone with local faults and the edges of former mining located over the end of the studied panel. This situation caused the occurrence of the last four analysed $M_L \geq 1.5$ events and the Benioff strain release changed into a new phase with an accelerating type of behaviour (days 370–460). The acceleration of the Benioff strain release resulted in characteristic steps which ended with a strong event. This phase also corresponded to an increase in seismic hazard level (Fig. 3) and to inelastic deformations in the roof-rocks (Fig. 5b). The end of mining on the day No. 460 was reflected in the flattened Benioff strain release curve due to the significant decrease in seismicity.

5. Conclusions

The spatiotemporal analysis of rock mechanics in roof-rocks is a complex phenomenon. The discussed results aimed to reveal the elastic or inelastic deformation during the excavation, as well as to use the energy-volume relation to assess if the strain energy in the rock mass was scattered or concentrated. The analyses provided information about the variation of the seismic hazard level, inelastic and elastic deformation, apparent volume, and Benioff strain release which changed in slope at each time interval of the longwall excavation. The study enabled three favourable conditions to be distinguished which were responsible for the increase in seismicity and seismic hazard. Moreover, the applied methods showed that comprehensive application of methods, i.e. seismic hazard assessment, calculations of apparent volume, and the energy-volume relation, can be a useful tool for analysing rock mechanic behaviour and the level of the strain–stress regime during underground mining operations. This study can also support other a preliminary geomechanical analysis which can impact on the mining factors generating seismic and rockburst hazard such as: mining method, roof control method, pattern of deposit cut, concentration of mining operations, and spatial limits of mining operations [31]. The presented spatiotemporal analysis confirms that the seismic energy released from the rock mass can be reasonably explained by the mechanical behaviour of the rock due to longwall mining. For instant, the other present works are also focused on a modelling of elastic strain energy transfer in pillars [32,33] or in roadways [34] resulting in rockburst or collapses in coal mines. This study introduced the concept of balanced seismic energy release during mining and its confirmation and application may reveal new possibilities of mining seismicity description and interpretation.

Acknowledgements

The authors would like to thank the Polish Mining Group that allowed the authors to publish the mining data and discuss the results. The authors would like to thank the reviewers for their thoughtful comments and efforts aimed at improving this paper.

References

[1] Lasocki S. Parametric or nonparametric analysis of induced seismicity sequences. In: Proceedings of the SPE/ISRM Rock mechanics in petroleum engineering conference 1994. Delft: Society of Petroleum Engineers; 1994.
[2] Davies R, Foulger G, Bindley A, Styles P. Induced seismicity and hydraulic fracturing for the recovery of hydrocarbons. Mar Pet Geol 2013;45:171–85.
[3] Wojtecki Ł, Mendecki MJ, Zuberek WM, Knopik M. An attempt to determine the seismic moment tensor of tremors induced by destress blasting in a coal seam. Int J Rock Mech Min Sci 2016;83:162–9.
[4] Leptokaropoulos K, Staszek M, Cielesta S, Urban P, Olszewska D, Lizurek G. Time-dependent seismic hazard in Bobrek coal mine, Poland, assuming different magnitude distribution estimations. Acta Geophys 2017;65(3):493–505.
[5] Lasocki S. Statistical distribution of seismological events. In: Guide for mining geophysicist. Kraków; 1995. p. 174–89.
[6] Convertito V, Maercklin N, Sharma N, Zollo A. From induced seismicity to direct time-dependent seismic hazard. Bull Seismol Soc Am 2012;102(6):2563–73.
[7] Mutke G, Dubiński J, Lurka A. New criteria to assess seismic and rock burst hazard in coal mines. Arch Min Sci 2015;60(3):743–60.
[8] Kijko A, Lasocki S, Graham G. Non-parametric seismic hazard in mines. Pure Appl Geophys 2001;158(9–10):1655–75.
[9] Lasocki S, Orlecka-Sikora B. Seismic hazard assessment under complex source size distribution of mining-induced seismicity. Tectonophysics 2008;456(1–2):28–37.
[10] Konicek P, Saharan MR, Mitri H. Destress blasting in coal mining – state-of-the-art review. Procedia Eng 2011;26:179–94.
[11] Gibowicz SJ, Kijko A. An introduction to mining seismology. San Diego: Academic Press; 1994.
[12] Lasocki S. Prediction of seismic hazard. In: Guide for mining geophysicist. Kraków; 1995.
[13] Konicek P, Soucek K, Stas L, Singh R. Long-hole destress blasting for rockburst control during deep underground coal mining. Int J Rock Mech Min Sci 2013;61:141–53.
[14] Konicek P, Schreiber J, Nazarova L. Volumetric changes in the focal areas of seismic events corresponding to destress blasting. Int J Min Sci Technol 2019;29(4):541–7.
[15] Wojtecki Ł, Konicek P. Estimation of active rockburst prevention effectiveness during longwall mining under disadvantageous geological and mining conditions. J Sustain Min 2016;15(1):1–7.
[16] Wojtecki Ł, Mendecki MJ, Zuberek WM. Determination of destress blasting effectiveness using seismic source parameters. Rock Mech Rock Eng 2017;50(12):3233–44.
[17] Wojtecki Ł, Konicek P, Mendecki MJ, Gołda I, Zuberek WM. Geophysical evaluation of effectiveness of blasting for roof caving during longwall mining of coal seam. Pure Appl Geophys 2019;177(2):905–17.
[18] Konicek P, Schreiber J. Rockburst prevention via destress blasting of competent roof rocks in hard coal longwall mining. J South Afr Inst Min Metall 2018;118(3):235–42.
[19] Aki K, Richards PG. Quantitative seismology: theory and methods. San Francisco: WH Freeman; 1980.
[20] Brune JN. Tectonic stress and the spectra of seismic shear waves from earthquakes. J Geophys Res 1970;75(26):4997–5009.
[21] Madariaga R. Dynamics of an expanding circular fault. Bull Seismol Soc Am 1976;66(3):639–66.
[22] Mendecki AJ. Seismic monitoring in mines. London: Chapman & Hall; 1997.
[23] Sagan G, Teper L, Zuberek WM. Tectonic analysis of mine tremor mechanisms from the upper Silesian coal basin. Pure Appl Geophys 1996;147(2):217–38.
[24] Kwiatek G, Martínez-Garzón P, Bohnhoff M. HybridMT: A MATLAB/shell environment package for seismic moment tensor inversion and refinement. Seismol Res Lett 2016;87(4):964–76.
[25] Wojtecki Ł, Mirek A, Dzik G. Edges of overlying seams as a factor responsible for strong mining tremors occurrence during underground hard coal extraction in the light of seismic moment tensor inversion method. In: Proceedings of the 5th international conference on applied geophysics. Ostrava: EDP Sciences; 2019.
[26] Lizurek G. Full moment tensor inversion as a practical tool in case of discrimination of tectonic and anthropogenic seismicity in Poland. Pure Appl Geophys 2017;174(1):197–212.
[27] Franke R. Scattered data interpolation: tests of some methods. Math Comput 1982;38(157):181–200.
[28] Davis JC. Statistics and data analysis in geology. New York: John Wiley and Sons; 1986.
[29] Dorugade AV. New ridge parameters for ridge regression. J Assoc Arab Univ Basic Appl Sci 2014;15(1):94–9.
[30] Mendecki MJ, Wojtecki Ł, Zuberek WM. Case studies of seismic energy release ahead of underground coal mining before strong tremors. Pure Appl Geophys 2019;176(8):3487–508.

[31] Małkowski P, Niedbalski Z. A comprehensive geomechanical method for the assessment of rockburst hazards in underground mining. Int J Min Sci Technol 2020;30(3):345–55.
[32] Wang F, Kaunda R. Assessment of rockburst hazard by quantifying the consequence with plastic strain work and released energy in numerical models. Int J Min Sci Technol 2019;29(1):93–7.
[33] Konicek P, Schreiber J. Heavy rockbursts due to longwall mining near protective pillars: a case study. Int J Min Sci Technol 2018;28(5):799–805.
[34] Song D, He X, Wang E, Li Z, Wei M, Mu H. A dynamic ejection coal burst model for coalmine roadway collapse. Int J Min Sci Technol 2019;29(4):557–64.